BIOCHEMISTRY
including biophysical chemistry & molecular biology

Article

pubs.acs.org/biochemistry

Terminal Interface Conformations Modulate Dimer Stability Prior to Amino Terminal Autoprocessing of HIV-1 Protease

Johnson Agniswamy,[†,§] Jane M. Sayer,[‡,§] Irene T. Weber,[†] and John M. Louis*[,‡,§]

[†]Department of Biology, Molecular Basis of Disease Program, Georgia State University, Atlanta, Georgia 30303, United States

[‡]Laboratory of Chemical Physics, National Institute of Diabetes and Digestive and Kidney Diseases, National Institutes of Health, DHHS, Bethesda, Maryland 20892, United States

ABSTRACT: The HIV-1 protease (PR) mediates its own release (autoprocessing) from the polyprotein precursor, Gag-Pol, flanked by the transframe region (TFR) and reverse transcriptase at its N- and C-termini, respectively. Autoprocessing at the N-terminus of PR mediates stable dimer formation essential for catalytic activity, leading to the formation of infectious virus. An antiparallel β-sheet interface formed by the four N- and C-terminal residues of each subunit is important for dimer stability. Here, we present the first high-resolution crystal structures of model protease precursor-clinical inhibitor (PI darunavir or saquinavir) complexes, revealing varying conformations of the N-terminal flanking ($S^{-4}FNF^{-1}$) and interface residues (P^1QIT^4). A 180° rotation of the T^4–L^5 peptide bond is accompanied by a new Q^2–L^5 hydrogen bond and complete disengagement of PQIT from the β-sheet dimer interface, which may be a feature for intramolecular autoprocessing. This result is consistent with drastically lower thermal stability by 14–20 °C of PI complexes of precursors and the mature PR lacking its PQIT residues (by 18.3 °C). Similar to the TFR-PR precursor, this deletion also results in a darunavir dissociation constant (2×10^4)-fold higher and a markedly increased dimer dissociation constant relative to the mature PR. The terminal β-sheet perturbations of the dimeric structure likely account for the drastically poorer inhibition of autoprocessing of TFR-PR relative to the mature PR, even though significant differences in active site–PI interactions in these structures were not observed. The novel conformations of the dimer interface may be exploited to target selectively the protease precursor prior to its N-terminal cleavage.

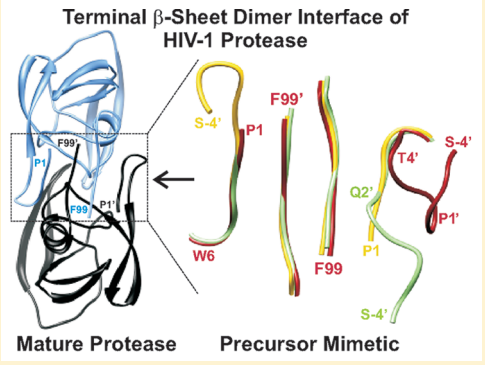

Sequential limited proteolysis of the virally encoded Gag and Gag-Pol polyprotein of HIV-1 (Figure 1) to mature structural and functional proteins is indispensable for precise assembly and propagation of infectious HIV.[1] This spatiotemporally regulated process is mediated by the virally encoded aspartyl protease.[1−3] In the Gag-Pol precursor the protease (PR) is flanked by the transframe region (TFR) and reverse transcriptase (RT) domains at its N- and C-termini, respectively (Figure 1). Upon release, the mature PR is composed of two 99-amino acid monomers, each contributing one of two catalytic aspartic acid residues.[2] In addition to the active-site dimer interface, the characteristic 4-stranded β-sheet interface comprising the N- and C-terminal residues contributes significantly to dimer stabilization and an intrinsically very low dimer dissociation constant (K_d).[2−4] Development of clinical protease inhibitors (PIs) binding to the active site of the mature PR has resulted in highly significant progress in the treatment of AIDS; however, the rapid evolution of PI resistant mutants under drug pressure presents a serious drawback to long-term treatment regimens.[5,6] Despite considerable efforts for developing an alternative approach to inhibit mature PR by targeting its terminal interface residues and disrupting the dimeric structure,[7,8] this approach has to date not produced any clinical applications, likely because of the extremely low K_d.

In contrast, precursor mimetics containing a truncated or the full-length transframe region (TFR) exhibit significantly higher K_d values accounting for their very low catalytic activity relative to the mature PR.[3] Self-cleavage (autoprocessing) of the precursor at the TFR-PR site is accompanied by the appearance of mature-like catalytic activity and stable dimer formation.[2,3] Initial steps in PR maturation depend, by necessity, on the intrinsic low catalytic activity of the precursor, which provides a regulatory mechanism to prevent premature release of the fully active PR prior to recruitment of the precursor at the plasma membrane.[2,9] This is consistent with our observation of transient dimer formation of the precursor detected by highly sensitive paramagnetic NMR.[10] Enzyme kinetics using model precursors have shown that the appearance of mature-like catalytic activity is linearly dependent on protein concentration, indicative of an intramolecular mechanism of cleavage.[2] Importantly, a mutation of this cleavage site leading to the accumulation of an N-terminally extended 17 kDa TFR-PR species causes a severe defect in Gag polyprotein processing and a complete loss of viral infectivity.[11] Two cleavages in Gag-

Received: December 8, 2011
Revised: January 6, 2012
Published: January 10, 2012

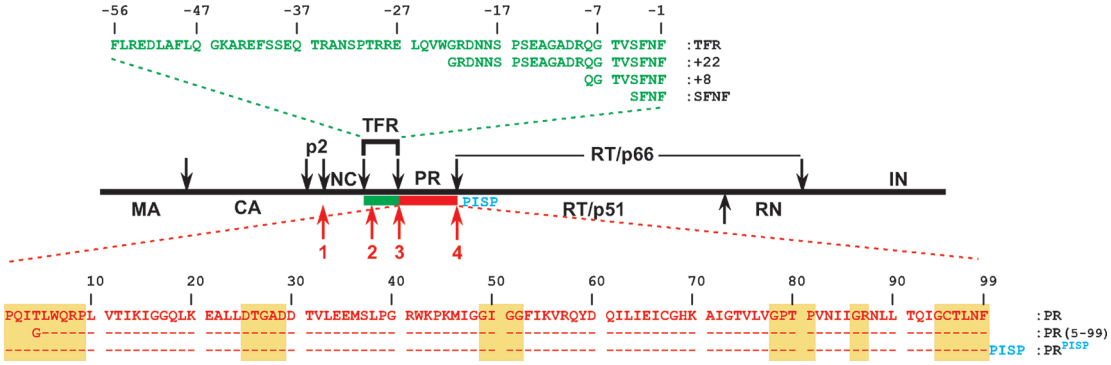

Figure 1. Structural organization of HIV-1 Gag-Pol polyprotein and sequences of PR constructs. The Gag-Pol polyprotein of HIV-1 is shown as a black line. Black arrows indicate sites cleaved by PR to release the mature proteins MA, matrix; CA, capisid; NC, nucleocapsid; RT, reverse transcriptase; RN, Rnase; and IN, integrase. Sequential processing sites, presumably occurring intramolecularly, leading up to the release of the PR at its N-terminus are shown by upward pointing red arrows (sites 1−3).[12,30] Site 4 cleavage occurs as a slower step subsequent to the cleavage at the N-terminus of PR.[2] Four residues (PISP) flanking the C terminus of PR (N-terminal residues of RT) are shown in blue. The green and red bars denote an optimized protease precursor mimetic TFR-PR[13] used extensively to study its maturation in *E. coli* and *in vitro*. Designations of constructs containing different lengths of the TFR, one truncation, and one C-terminal extension of PR are indicated. PR in all constructs bears the mutations Q7K, L33I, L63I, C67A, and C95A, the first 3 to restrict autoproteolysis and the latter 2 to avoid cysteine−thiol oxidation.[3] The truncated construct PR(5−99) is less stable as a dimer than PR because it lacks the four N-terminal residues (PQIT) contributing to the β-sheet dimer interface from both subunits. It constitutes an extreme model for a conformer of the precursor mimetic ^{SFNF}PR, observed in crystal structures reported here, in which half of these interactions are lost by disengagement of one N-terminal strand from the β-sheet. Yellow highlights depict the highly conserved regions in PR.[3,13]

Pol, first at the p2/NC site and subsequently between residues F^{-49} and L^{-48} near the N-terminus of TFR, are suggested also to occur intramolecularly prior to the cleavage at the N-terminus of PR (sites marked 1−3 in Figure 1).[2,12] However, the drastic shift to a stable dimer associated with mature-like catalytic activity occurs only upon TFR/PR cleavage (site 3).[2] These cleavages precede the intermolecular cleavage at the C-terminus of PR (PR/RT, site 4)[2] and the rest of the Gag and Pol sites. The latter cleavages are predicted to occur intermolecularly mediated by the fully active mature PR.

TFRs from the four groups of HIV (M, N, O, and P) range in length from 52 to 61 amino acids.[13] The exact structural role of TFR in modulating protease function is not fully known. Isolated TFR exhibits no specific structure.[14] Even though *in vitro* viral replication is tolerant to large deletions and substitutions within TFR, a large nonnative sequence insertion was shown to interfere with maturation and virus production, suggesting that overall length of TFR may be critical for its function.[15] It is noteworthy that both the terminal regions of TFR are pH-dependent competitive inhibitors when added to the mature PR while inhibition by TFR lacking its C-terminal residues SFNF, which form half of the TFR/PR cleavage site, was significantly reduced.[16] Structural and biophysical characterizations of PR precursors until recently have been impractical because intrinsic autoprocessing upon expression in *E. coli* leads to very poor accumulation and insufficient yields of pure protein. We recently reported[13] a methodology to inhibit precursor maturation in *E. coli* by PIs added to the culture medium, thereby permitting assessment of binding affinities of PIs to precursors as well as their accumulation and purification. Although darunavir (DRV) and saquinavir (SQV) were the best inhibitors of N-terminal autoprocessing among the PIs, they surprisingly showed very poor inhibitory potencies (IC_{50} of ∼1−2 μM), which is 2−5 orders of magnitude larger than their K_i values for binding to mature PR. In mammalian cells, N-terminal autoprocessing of a chimeric construct containing TFR-PR also exhibited a similar weak response to inhibition by DRV (IC_{50} ∼ 1.5 μM).[17]

As full-length TFR-PR precursor-PI complexes do not effectively crystallize, we used a surrogate of the precursor in which the PR is flanked by SFNF. ^{SFNF}PR exhibits properties similar to those of TFR-PR in terms of thermal stability and dimer dissociation. Here we present the crystal structures of ^{SFNF}PR in complex with a PI to prevent autoprocessing. These high-resolution structures reveal distinct conformations of the flanking SFNF residues and alternate conformations of the N-terminal PQIT residues of PR. The effects of N- or C-terminal flanking sequences and the deletion of the N-terminal PQIT residues on the thermal stability of PR−PI complexes are also analyzed. These results are interpreted in conjunction with the structural data, and possible intermediate conformations of the β-sheet interface residues that may permit intramolecular autoprocessing are discussed. In addition, these findings may provide a structural basis to target the PR prior to its maturation from the Gag-Pol precursor.

MATERIALS AND METHODS

Protease Constructs and Protein Preparations. Gene manipulations were carried out as described.[13] Constructs used in this study are listed in Figure 1. Protease constructs were cloned in pET11a vector and expressed in *E. coli* BL21(DE3). To allow isolation of sufficient quantities of purified precursor proteins for structural and calorimetric studies, cultures were scaled up to a total volume of 100 mL in the presence of PI. Proteins were purified from inclusion bodies and folded as described.[18,19]

Differential Scanning Calorimetry. Measurements were performed using a MicroCal VP-DSC microcalorimeter as described.[20] Because the precursor constructs undergo rapid autoprocessing in the absence of inhibitors, all experiments were conducted in the presence of ∼2-fold molar excess of DRV relative to dimeric protein. Precursors were folded by addition of 5.66 volumes of 5 mM sodium acetate buffer, pH 6, containing DRV inhibitor, to 1 volume of ∼2 mg/mL protein in 12 mM HCl, to give final protein concentrations of 9−15 μM dimer and a final pH of 4.5−5.0. Mature PR was prepared

in a similar manner. Thermal scans were begun at 20 or 25 °C and run at a rate of 90 °C/h to a final temperature of 85−95 °C, depending on the observed T_m. Data were processed as described previously. Values of the T_m were determined from the maxima of the transitions.

Isothermal Titration Calorimetry of PR(5−99) with DRV. PR(5−99) in 12 mM HCl was folded by the quench protocol as described[19] to give a final buffer concentration of 50 mM sodium acetate, pH 5, and DMSO was added to give a final concentration of 0.18% in 350 μL. The sample was titrated with 15 2.45 μL aliquots of 106 μM DRV in a buffer of the same composition using a MicroCal high-precision iTC$_{200}$ microcalorimeter (GE Healthcare). Time intervals between injections were manually adjusted from an initial value of 180 s to a final value of 300 s to compensate for increasing peak broadening as the titration progressed. The protein concentration as dimers was estimated to be 6.8 μM based on the titration end point, the known concentration of DRV, and a stoichiometry of 1:1 for inhibitor binding. Data were analyzed using the instrument's Origin software. SDS-PAGE before and after titration indicated the presence of a single band corresponding to PR(5−99) with no degradation products.

Crystallization, Data Collection, Structure Determination, and Refinement. Proteins were folded in the presence of inhibitor to prevent autoprocessing. The crystals of ^{SFNF}PR/DRV complex were grown in hanging drops at room temperature against a reservoir solution of 0.6 M sodium chloride, 0.1 M sodium citrate at pH 5.5. Crystals of ^{SFNF}PR/SQV and ^{SFNF}PR/SQV$_{2dimer}$ complexes were grown using reservoir solutions of 0.4 M sodium chloride, 0.1 M sodium cacodylate at pH 6.0 and 0.65 M ammonium chloride, 0.1 M sodium acetate at pH 4.8, respectively. Crystals were cooled in liquid nitrogen in the presence of 30% glycerol cryoprotectant. Diffraction data at 100 K were collected on beamline 22-ID of the Southeast Regional Collaborative Access Team (SER-CAT) at the Advanced Photon Source, Argonne National Laboratory. The data were integrated and scaled with HKL2000.[21] Structures of the ^{SFNF}PR/DRV and ^{SFNF}PR/SQV complexes were solved by molecular replacement employing PHASER,[22,23] with the PR/DRV (2IEN)[24] and PR/SQV (3OXC)[25] structures, respectively, as starting models. N-terminal residues 1−4 of the models were pruned during molecular replacement and remodeled during refinement. Structures were refined using SHELX-97,[26] and model building was performed in COOT.[27] Solvent molecules were inserted at stereochemically reasonable positions using $2F_o-F_c$ and F_o-F_c maps at 1σ and 3σ levels, respectively. The final refined structures have no disallowed ϕ/ψ values on the Ramachandran plot in Procheck.[28] Molecular representations were prepared with Chimera[29] and PyMOL. Single crystals were collected, rinsed 2 times with buffer containing DRV, dissolved in 8 M urea, and then subjected to ESI-MS to verify the intactness of ^{SFNF}PR.

RESULTS AND DISCUSSION

Influence of N-Terminal TFR Residues on the Thermal Stability of Precursor Dimer−PI Complexes. As the cleavage at the N-terminus of PR precedes the C-terminal cleavage, PR flanked by the N-terminal TFR represents a good model for structural and biophysical studies prior to autoprocessing. It is impractical to study the PR precursor in the absence of inhibitor *in vitro* as it undergoes autoprocessing to the mature PR immediately upon folding.[2] However, DSC in the presence of PI to prevent autoprocessing provides a sensitive measure of the combined dimer stability and inhibitor binding affinity of a dimer−PI complex. Consistent with weaker binding of DRV to the TFR-PR precursor, the thermal melting of the TFR-PR/DRV complex (Figure 2 and Table 1) indicates

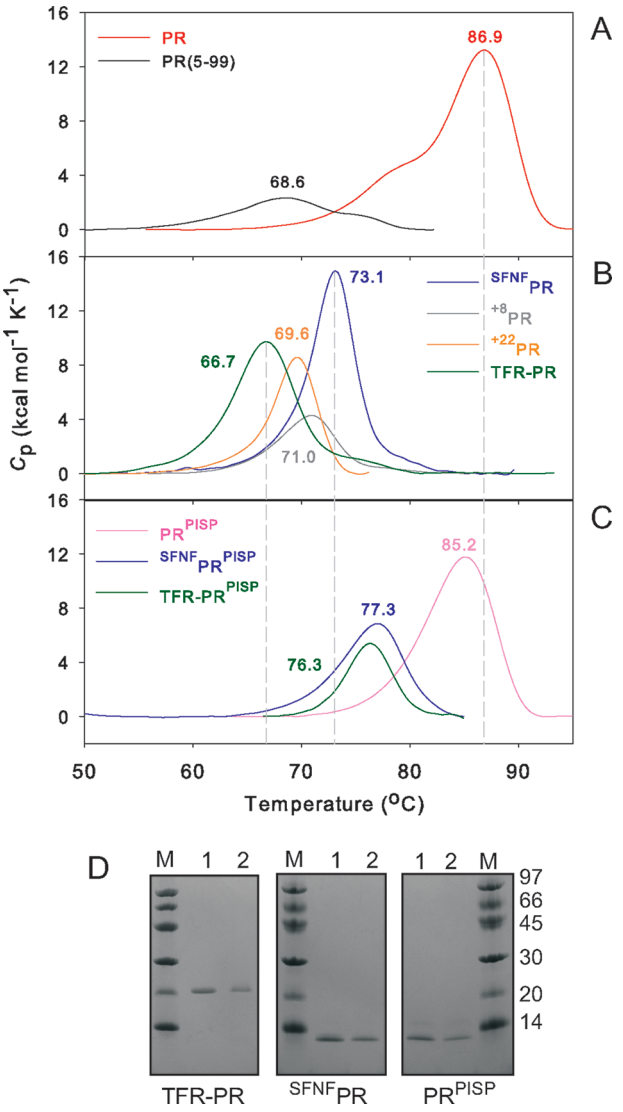

Figure 2. Influence of sequences at the N-terminal interface and those flanking the PR on thermal stability in the presence of DRV (A, B, and C). DSC scans were performed in 5 mM sodium acetate, pH 4.5−5, in the presence of a ∼2-fold molar excess of DRV relative to the proteins (as dimers). The T_m value is indicated at the maximum of each transition. The decrease in T_m relative to mature PR/DRV (ΔT_m)[13] provides a semiquantitative assessment of the destabilization of the dimer/DRV complexes of PR precursor mimetics and PR deletion mutant. The DSC thermogram for TFR-PR is included solely for comparison in (B).[13] (D) Gel analysis of proteins subjected to DSC. Representative analysis of folded precursor mimetics (∼10 μM) by SDS-PAGE on 20% homogeneous PhastGels prior to (lane 1) and after DSC (lane 2) in the presence of DRV to verify inhibition of autoprocessing/protein degradation. Bands were visualized by Coomassie staining. M denotes markers in kDa.

a 20.2 °C decrease in the T_m relative to the PR/DRV complex (86.9 °C). Addition of as few as 4 amino acids of TFR (SFNF) also strikingly decreases the thermal stability of a ternary complex. ^{SFNF}PR exhibits a T_m decrease of 13.8 °C, corresponding to ∼70% of the decrease observed with the

dx.doi.org/10.1021/bi201809s | *Biochemistry* 2012, 51, 1041−1050

Table 1. Effect of N- and C-Terminal Flanking Sequences on Thermal Stability of PR Precursor/DRV Complexes

construct	T_m[a] (°C)	ΔT_m[b] [vs PR (°C)]	ΔT_m[c] [vs PR^{PISP} (°C)]	ΔH_{app}[a] (kcal/mol)
PR	80.4, 86.9			54.4, 75.2
PR(5−99)	68.6	18.3		27.6
^{SFNF}PR	73.1	13.8		88.5
$^{+8}$PR	71.0	15.9		31.5
$^{+22}$PR	69.6	17.3		48.1
TFR-PR	66.7	20.2		77.0
PR^{PISP}	85.2	1.7		95.3
$^{SFNF}PR^{PISP}$	77.3	9.6	7.9	52.7
TFR-PR^{PISP}	76.3	10.6	8.9	29.9

[a]Values for minor and major peaks are indicated. [b]Major T_m of PR − T_m of the specified construct. [c]T_m of PR^{PISP} − T_m of the specified construct.

56-residue TFR. Extensions of 8 and 22 amino acids ($^{+8}$PR and $^{+22}$PR) give intermediate values of T_m. These results are consistent with an earlier observation by NMR that ^{SFNF}PR with an added effect of an active site D25N mutation, which also influences dimerization, is mainly monomeric in the absence of inhibitor ($K_d \sim 0.5$ mM).[3]

Apparent enthalpy (ΔH_{app}) values determined by integration of the thermal transition peaks are summarized for qualitative comparison in Table 1. However, the inability of PR and its PI complexes to undergo a reproducible second scan at optimal pH conditions for catalytic activity[20] precludes quantitative thermodynamic analysis. Unlike the T_m values, which are related to overall stability of the complexes, the enthalpy values do not follow the same trend (Figure 2B). It is possible that unusually small enthalpy values (such as for $^{+8}$PR) may be offset by large entropic effects. Evaluation of the relative contributions of these factors will depend on future detailed structural information.

It is noteworthy that complexes of mature PR with several tight binding PIs exhibit biphasic DSC transitions,[20] whereas weaker binding inhibitors do not show this effect. Possible causes of biphasic transitions include (1) occupancy by the PI of two orientations in the active site or (2) partial unfolding of the PR, followed by dissociation of the PI coupled with complete unfolding. For weaker complexes or PR constructs that are dimeric only when stabilized as such by inhibitor binding, including the present precursor mimetics, PI dissociation at temperatures above the T_m of the monomer is likely simultaneous with dimer dissociation and monomer unfolding.

Measuring the K_d of active ^{SFNF}PR is not feasible kinetically by following the dependence of enzymatic activity on protein concentration because of autoprocessing, but ^{SFNF}PR is expected to exhibit an increased dimer stability by ~100-fold more than ^{SFNF}PR(D25N) based on earlier work comparing the K_d's of the mature PR (<10 nM) and PR(D25N) (~1 μM).[20] Thus, as TFR-PR precursor−PI complexes did not form crystals of suitable quality, active ^{SFNF}PR provides a simple realistic model to explore the structural basis for the decreased dimer stability and the weaker binding of PIs to the PR precursor.

Crystal Structures of ^{SFNF}PR Precursor−PI Complexes. Active precursor proteins form dimers in the presence of tight binding PIs,[3] thus preventing the protein from undergoing autoprocessing during crystallization studies. We describe three crystal structures revealing four independent conformations of ^{SFNF}PR dimer in complexes with DRV or SQV. The ^{SFNF}PR/DRV crystals belong to orthorhombic space group $P2_12_12$ with one dimer spanning residues Ser-4 to Phe99 and Ser-4′ to Phe99′ per asymmetric unit. The presence of the intact ^{SFNF}PR was further confirmed by subjecting the dissolved crystals to ESI-MS (mass of 11223). The SQV complexes crystallized in two orthorhombic space groups, $P2_12_12$ and $P2_12_12_1$, with one and two ^{SFNF}PR dimers per asymmetric unit, respectively. The structures were refined to resolutions of 1.32−1.55 Å and *R*-factors from 16 to 16.4% (crystallographic statistics are listed in Table 2).

Table 2. Crystallographic Data Collection and Refinement Statistics

	^{SFNF}PR/DRV	^{SFNF}PR/SQV	$^{SFNF}PR/SQV_{2dimer}$
PDB code	3TKW	3TL9	3TKG
space group	$P2_12_12$	$P2_12_12$	$P2_12_12_1$
cell dimensions			
a (Å)	59.32	59.41	80.07
b (Å)	86.22	86.10	88.94
c (Å)	45.95	46.10	60.17
molecules/asymmetric unit	1	1	2
resolution range (Å)	50.0−1.55	50.0−1.32	50.0−1.36
total observations	224 087	291 134	578 537
unique reflections	34 602	51 505	87 215
redundancy	6.5 (4.2)	5.7 (2.0)	6.6 (3.1)
completeness	99.0 (92.4)[a]	91.4 (53.2)	93.5 (59.7)
$\langle I/\sigma(I)\rangle$	25.9 (3.4)	26.1 (2.1)	34.1 (2.6)
R_{sym} (%)	6.3 (44.9)	5.7 (41.3)	4.9 (45.9)
refinement resolution range (Å)	10−1.55	10.0−1.32	10.0−1.36
R_{cryst} (%)	16.4	16.1	16.0
R_{free} (%)	23.1	20.4	21.4
no. of solvent molecules	133	165	260
mean *B*-factor (Å^2)	30.1	22.9	22.9
rms deviations from ideality			
bond length (Å)	0.01	0.01	0.01
angles (Å)[b]	0.03	0.04	0.03
relative occupancy of inhibitor	0.51/0.49	0.61/0.39	0.69/0.31, 0.54/0.46

[a]Values in parentheses are given for the highest resolution shell (^{SFNF}PR/DRV: 1.58−1.55 Å; ^{SFNF}PR/SQV: 1.37−1.32 Å; $^{SFNF}PR/SQV_{2dimer}$: 1.41−1.36 Å). [b]The angle rmsd in SHELX97[26] is indicated by distance in Å.

Except for the N-terminus, the overall structures of ^{SFNF}PR complexes, including the conformation of flaps and the inhibitor binding site, are similar to those of the mature PR complexes (Figure 3). The ^{SFNF}PR/DRV and ^{SFNF}PR/SQV complexes with a single dimer can be superimposed with those of the corresponding mature PR complexes 2IEN[24,25] and 3OXC[24,25] with rmsd values of 0.32 and 0.65 Å for 190 Cα atoms excluding the first four N-terminal residues (PQIT) of PR. The two dimers in $^{SFNF}PR/SQV_{2dimer}$ superimpose with the mature PR/SQV complex[25] with rmsd values of 0.56 and 0.59 Å for 190 Cα atoms. All four structures are superimposed as shown in Figure 3D.

Dimer Interfaces. A prominent stabilizing feature of the dimer interface in the mature PR is the 4-stranded antiparallel β-sheet in which two outer N-terminal strands sandwich the

dx.doi.org/10.1021/bi201809s | *Biochemistry* 2012, 51, 1041−1050

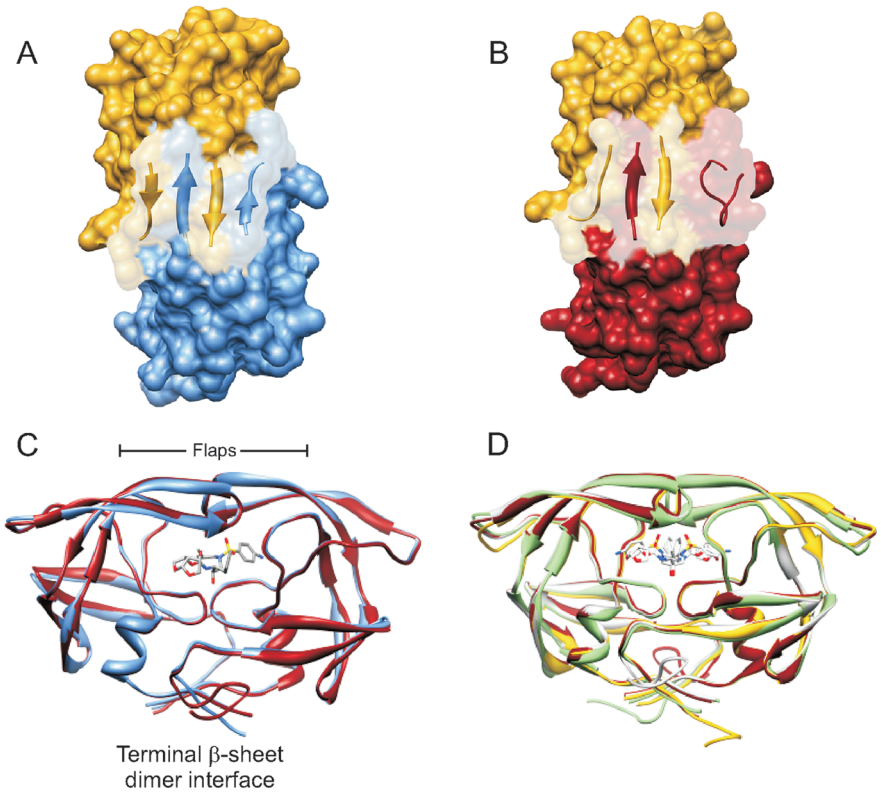

Figure 3. Overall structural comparison of ^{SFNF}PR and PR inhibitor complexes. Surface representations of PR/DRV (A, 2IEN,[24] monomers in gold and blue) and ^{SFNF}PR/DRV (B, monomers in gold and dark red). Terminal β-sheet interface orientations are shown as ribbons on the surface representations. (C) Ribbon overlay of these two structures with a stick representation of DRV bound in one orientation to the active site. (D) Four independent structures of ^{SFNF}PR determined in this study with a stick representation of DRV bound in two orientations to the active site: ^{SFNF}PR/DRV (dark red, space group $P2_12_12$), ^{SFNF}PR/SQV (light gray, space group $P2_12_12$), and ^{SFNF}PR/SQV$_{2dimer}$ (yellow and light green, space group $P2_12_12_1$).

two C-terminal strands (Figures 3 and 4). The four different dimers of ^{SFNF}PR resemble the mature PR, except for the conformational changes in the N-terminal residues associated with the flanking SFNF residues. Residues Ser-4 to Thr4 disengage in four distinct conformations as illustrated in Figures 3D and 4A. In both single dimer ^{SFNF}PR/DRV and ^{SFNF}PR/SQV complexes, the N-terminal residues Pro1′ to Thr4′ (corresponding to the N-terminus of mature PR) of monomer B exhibit alternate conformations with 0.7 (major) and 0.3 (minor) occupancies (Figure 5A,B). We note the existence of residual density suggesting the possibility of additional disordered conformations. In the major conformation, residues Pro1′ to Thr4′ of monomer B detach from the β-sheet and lose three hydrogen bond interactions with the C-terminal residues including the interaction between the terminal Pro1 and Phe99′ residues, which is characteristically an ion pair for the free termini in the mature PR. This unraveling results in a 3-stranded β-sheet instead of the typical 4-stranded sheet observed for the mature PR (Figure 4B,C). Weaker density is seen for the minor conformation of residues Pro1′ to Thr4′, which retain the mature 4-stranded β-sheet conformation (Figure 5A,B), although no polar interaction occurs between Pro1′ and Phe99, unlike in the mature PR. The flanking N-terminal residues SFNF are visible in the electron density maps for the major but not the minor conformation. A salient feature of the major conformation is the peptide bond between Thr4′ and Leu5′, which flips by 180° to facilitate the formation of a β-turn with a hydrogen bond between main chain atoms of Gln2′ and Leu5′ (Figures 5A,B and 6A). The β-turn facilitates the disengagement and fraying of residues Pro1′ to Thr4′ from the terminal β-sheet. Phe-1′, the first residue flanking the PR, inserts into the hydrophobic pocket occupied by the side chain of Ile3′ in the mature PR and interacts with the hydrophobic side chains of Ile3′, Pro9′, Val11′, Leu24′, Leu97, and Phe99 at the dimer interface (Figure 6B). Ile3′ is displaced by the formation of the β-turn in ^{SFNF}PR/DRV and ^{SFNF}PR/SQV and lacks hydrophobic interactions seen at the interface in mature PR; instead, Ile3′ forms a new contact with Thr96. Also, unusual alternate conformations were revealed for the side chain of Trp6′ with relative occupancy of 0.7/0.3 and 0.51/0.49 in the ^{SFNF}PR/DRV and ^{SFNF}PR/SQV complexes, respectively, unlike the majority of mature PR structures. In monomer A of ^{SFNF}PR/DRV and ^{SFNF}PR/SQV complexes, the conformation of the N-terminal residues resembles that of the mature PR as part of the typical 4-stranded β-sheet albeit at lower occupancies. Weak residual electron densities were apparent for the frayed conformation but were not modeled. Likewise, it was not possible to model unambiguously the N-terminal flanking sequence in monomer A. The conformation of flanking residues in monomer A cannot be the same as that of monomer B due to crystal contacts in that region. The observed disorder around the flanking residues in both monomers A and B suggests the existence of multiple conformations. Interestingly, the major conformation showing a complete disengagement of the N-terminal residues is consistent with our earlier NMR observation that an inactive ^{SFNF}PR precursor, bearing a D25N mutation to preclude autoprocessing, exhibited chemical shift perturbations of its N-

dx.doi.org/10.1021/bi201809s | *Biochemistry* 2012, 51, 1041−1050

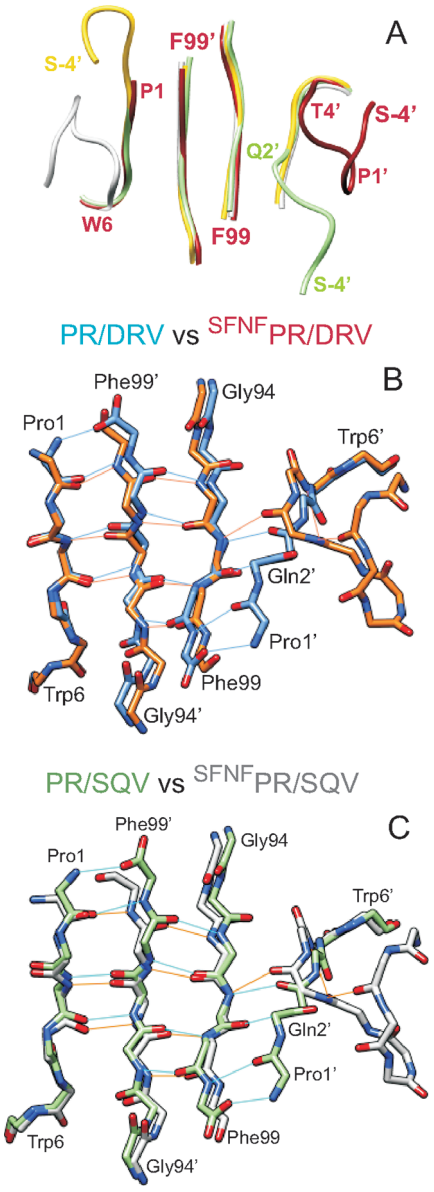

Figure 4. Terminal interface conformations. (A) Alignment of the four dimers (shown in Figure 3D) to visualize the different backbone conformations of the N-terminal flanking residues. Residue positions are marked using colors matching those of the structures in 3D. (B, C) Comparison of the hydrogen bond network at the terminal β-sheet interface of major conformations of ^{SFNF}PR [orange (DRV) and white (SQV) sticks] and PR [blue (DRV) and green (SQV) sticks] bound to PI. H-bonds are shown in orange for ^{SFNF}PR and in blue for PR. Peptide bond O and N atoms are colored red and dark blue, respectively. Residues Thr4′ to Pro1′ have different conformations in ^{SFNF}PR and PR.

terminal residues 3−6, possibly resulting from their interaction with the SFNF extension.[19]

In the ^{SFNF}PR/SQV$_{2dimer}$ crystal structure, the interfacial 4-stranded β-sheet is largely intact in both dimers (Figure 4A, yellow and green strands), except for the the polar interaction between the N- and C-termini seen in the mature PR due to rearrangement of Pro1 associated with the SFNF extension (as in Figure 3B,C). The N-terminal SFNF extension is not visible in the electron density for monomer B of either dimer. However, this extension is clearly visible with unambiguous electron density in monomer A of both dimers (Figure 5C). The conformation of the N-terminal extension differs in the two dimers and may be partly influenced by crystal lattice contacts, whereas this region lacks crystal contacts in single dimer ^{SFNF}PR/DRV and ^{SFNF}PR/SQV complexes. In monomer A of dimer-1, the N-terminal extension bends after Phe-1 and forms a turn exhibiting extensive crystal contacts. In monomer A of dimer-2, the Phe-3 side chain protrudes into a similar interfacial hydrophobic pocket as the Phe-1 of ^{SFNF}PR/DRV and ^{SFNF}PR/SQV complexes and forms extensive hydrophobic interactions with surrounding side chains (Figure 6C). Interestingly, Phe99′ forms intersubunit aromatic interactions with Phe-3 in ^{SFNF}PR/SQV$_{2dimer}$ and Phe99 with Phe-1′ in single dimer crystal structures (Figure 6B).

Inhibitor Interactions. The inhibitors DRV and SQV are bound at the active site in ^{SFNF}PR complexes with no significant conformational changes in the binding site, and they retain all hydrogen bond interactions observed in the corresponding mature PR complexes (Figure 7A,B). DRV and SQV bind in two orientations related by 180° in both ^{SFNF}PR and mature PR complexes. The relative occupancies of the inhibitors vary from 0.5/0.5 to 0.7/0.3, as listed in Table 2. The central hydroxyl group of both inhibitors interacts closely with the carboxylates of the two catalytic residues Asp25 and 25′. Both inhibitors form conserved water-mediated hydrogen bonds with the amides of Ile50 and 50′ at the flap tips. In addition, SQV forms direct hydrogen bonds with main chain atoms of Asp29, Asp30, and Gly48 in one monomer, while DRV forms seven hydrogen bonds with residues Gly27′ and Asp29 and Asp30 in both monomers. Notably, even the side chain and main chain conformations of residues in the inhibitor binding sites are similar for ^{SFNF}PR and mature PR complexes. However, highly similar binding modes revealed by crystal structures do not always correlate with binding affinities for tight binding inhibitors. For example, the interactions of DRV with the inactive mature PR$_{D25N}$ were almost indistinguishable from those with PR in the crystal structures even though this active site mutation results in ~10^6-fold decreased affinity for DRV.[20] We speculate that structures complexed with weaker binding inhibitors than DRV and SQV or with substrate analogue inhibitors may reveal differences in inhibitor interactions with the PR precursor relative to the mature PR, as inhibitor induced stabilization at the active site is minimized.

Effect of Deleting the N-Terminal Residues 1−4 of Mature PR on Dimerization and PI Affinity. Several properties of PR precursors are consistent with our present observation of disengagement of a segment of the N-terminal sequence from the β-sheet interface. These include markedly increased K_d values for dimer dissociation,[3] much poorer inhibition by active-site directed PIs,[13] and decreased thermal stability of ternary dimer−PI complexes (this work), which presumably reflects contributions of both weaker inhibitor binding and lower dimer stability. The observed conformations are mechanistically reasonable; presumably more extensive unraveling of the N-terminal sequence would be required to permit the N-terminal cleavage site (SFNF/PQIT) to reach into the active site of the same transient dimer for intramolecular N-terminal autoprocessing, as evidenced by kinetics.[2] The N-terminal sequence must unravel up to about Pro9 to facilitate ~18 Å movement of the cleavage site toward the catalytic aspartates of the same transient dimer. The extended unraveling of the N-terminal sequence will likely perturb the intermonomer ion pair between Arg8 and Asp29′. This interaction affects the K_d and catalytic activity minimally as

dx.doi.org/10.1021/bi201809s | *Biochemistry* 2012, 51, 1041−1050

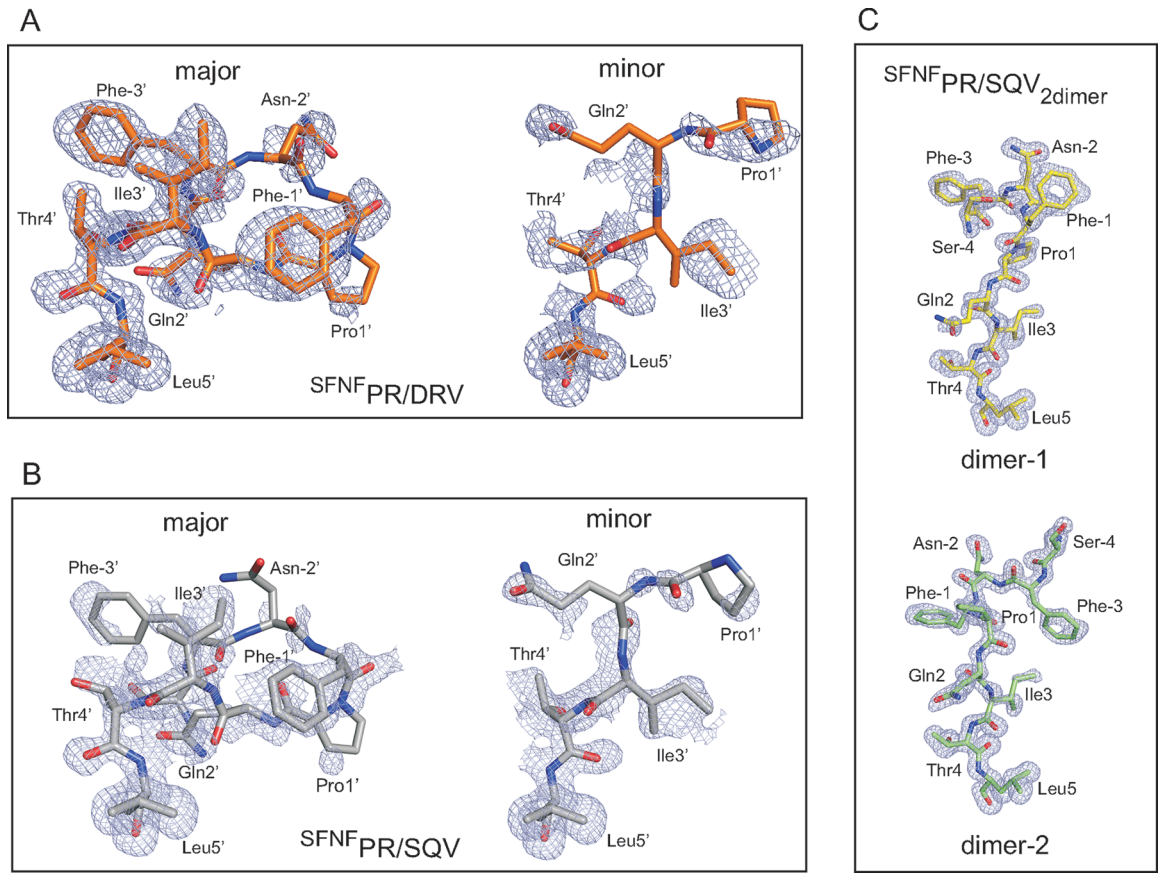

Figure 5. F_o-F_c electron density maps. (A, B) Major conformations of disengaged N-terminal residues (Leu5′ to Ser-4′) in ^{SFNF}PR/DRV and ^{SFNF}PR/SQV contoured at 2.5σ. Minor conformations (Leu5′ to Pro1′) in ^{SFNF}PR/DRV and ^{SFNF}PR/SQV contoured at 2.5σ. (C) N-terminal residues (Leu5 to Ser-4) in dimer-1 and dimer-2 of ^{SFNF}PR/SQV$_{2dimer}$ contoured at 3σ.

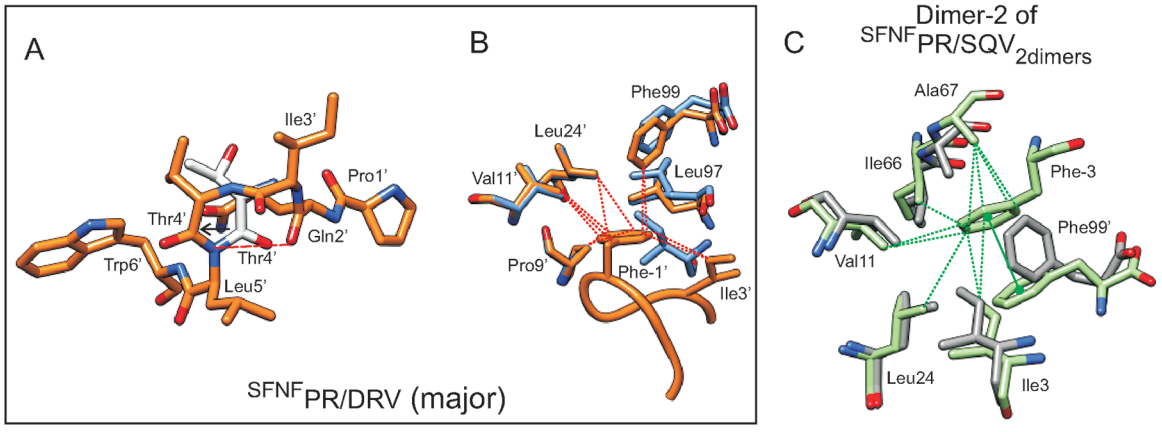

Figure 6. Altered interactions of the N-terminal residues of ^{SFNF}PR. (A) The disengaged N-terminal residues of ^{SFNF}PR/DRV (major conformation) form a β-turn between Ile3′ and Thr4′ characterized by a hydrogen bond between Gln2′ and Leu5′. Both conformations of Thr4′ are shown with the minor conformation shown in white. The black arrow indicates a 180° rotation of the peptide bond between Thr4′ and Leu5′. (B) Phe-1′ side chain of N-terminal extension in ^{SFNF}PR/DRV (major conformation) lies in the hydrophobic pocket partially replacing Ile3′ of PR/DRV. Hydrophobic interactions are shown as dotted lines. (C) The hydrophobic interactions of Phe-3 of N-terminal extension in dimer-2 of ^{SFNF}PR/SQV$_{2dimer}$ represented by dotted lines. The aromatic side chains of Phe-3 and Phe99′ stack against each other as indicated by a solid green line. PR/SQV (3OXC)[25] is overlaid in gray for comparison.

shown by mutagenesis.[30] The limited disengagement of only a few N-terminal residues could be a forced consequence of enhanced dimer stabilization by PI interacting with the active site and flap residues, and further disengagement might occur in the absence of PI and/or with a longer, unstructured N-terminal TFR. However, neither of these possibilities has been amenable to demonstration by crystallography since PIs must be used to suppress the rapid autoprocessing of folded precursor, and the TFR−PR-PI complexes did not form suitable crystals. The possibility that the N-terminal sequence downstream to residues 1−4 can become unstructured without complete unfolding of the rest of the (monomeric) PR

dx.doi.org/10.1021/bi201809s | *Biochemistry* 2012, 51, 1041−1050

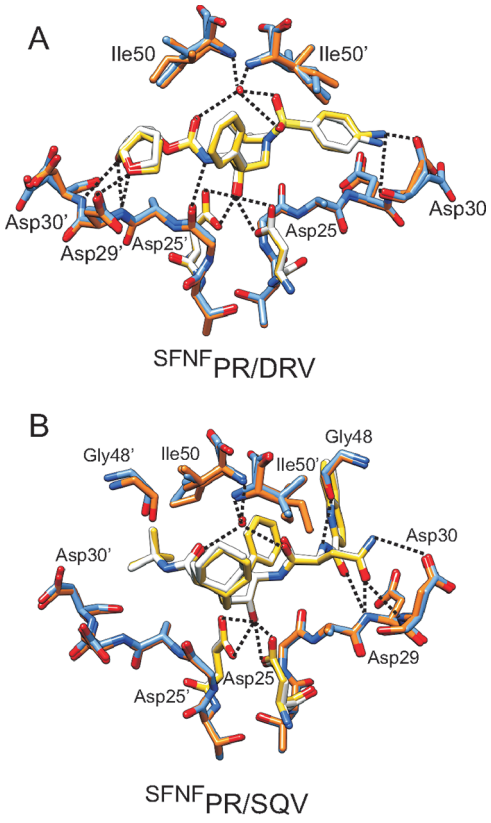

Figure 7. Inhibitor interactions in ^{SFNF}PR and PR. Comparison of the hydrogen bond interactions of DRV (A) and SQV (B) in the active site of ^{SFNF}PR (orange) and PR (blue) in the major conformation. DRV and SQV bound to ^{SFNF}PR and PR are shown overlaid in yellow and white, respectively. Active site residues (D25) of ^{SFNF}PR and PR are also depicted in yellow and white, respectively.

molecule is supported by our earlier results that although C-terminal residues 96−99 are indispensable for dimer formation even in the presence of PI,[3] solution NMR analysis of the PR monomer spanning residues 1−95 reveals a tertiary fold for residues 10−90, with the N-terminal 1−9 and C-terminal 91−95 residues exhibiting no specific structure.[3] Consistent with this observation, while P1A, Q2A, and T4A mutations were tolerated, C-terminal T96A, L97A, and F99A substitutions led to significantly reduced activity.[31] It has been shown that mutations affecting RT dimerization impair PR-mediated Gag-Pol processing.[32,33] A drug that promotes RT dimer formation has also been linked to enhanced processing of a model Gag-Pol precursor by PR.[34] We suggest that RT dimerization together with interactions of the C-terminal PR residues 96−99 may play a role in initiating N-terminal autoprocessing.

As autoprocessing of the precursors precludes use of active, folded TFR-PR or ^{SFNF}PR in the absence of inhibitor, we used a deletion mutant, PR(5−99), which lacks N-terminal interactions in the β-sheet interface, to mimic the loss of these interactions in the PR precursor. PR(5−99) represents an extreme example, since the deletion affects both monomers, such that almost half of the 4-stranded β-sheet interactions essential for stable dimer formation are absent. By contrast the disengagement of the N-terminus is seen to affect only one monomer in ^{SFNF}PR, and furthermore the observation of several different conformations for this precursor mimetic is consistent with an ensemble of conformations with and without N-terminal disengagement. The deletion has been shown by NMR to increase the extent of dimer dissociation to folded monomers markedly[3] with a K_d for dimer dissociation of ~300 nM by enzyme kinetics (K_d for PR is <10 nM), closer to the value estimated for TFR-PR.[3,30] The deletion also markedly decreases the thermal stability of PR(5−99) as its DRV complex to about the same extent as a flanking TFR sequence (Figure 2A and Table 1) but more than the SFNF sequence, an observation that suggests that the full length TFR may have a slightly greater effect on the β-sheet interface. Consistent with this observation, calorimetric titration of PR(5−99) with DRV (Figure 8) gave a dissociation constant for the PI of 190 nM,

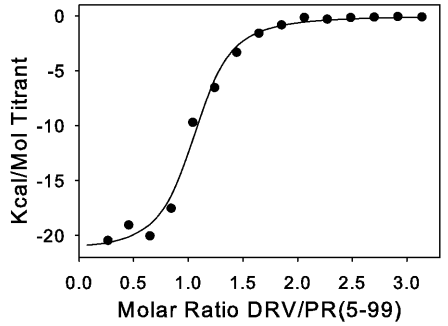

Figure 8. ITC titration of deletion mutant PR(5−99) with DRV at pH 5. Curve fitting of the data gave an association constant of (5.4 ± 1.4) × 10^6 M^{-1}, corresponding to an inhibitor K_i of 190 nM.

which is ~4 orders of magnitude weaker than its binding to PR, but not extremely different (~5-fold) from the IC_{50} of 1 μM for inhibition of TFR-PR maturation.[13]

Effect of C-Terminal Flanking Residues on Thermal Stability. Precursor constructs bearing a four-residue C-terminal flanking sequence (PISP) derived from the N-terminus of RT, in addition to the N-terminal extension, provide a model to mimic the environment of the PR domain within the Gag-Pol. However, attempts to crystallize ^{SFNF}PR^{PISP} or PR^{PISP} or its active site mutant forms bearing the D25N mutation, all as ternary complexes in the presence of DRV, were unsuccessful. Consequently, we assessed the effects of C-terminal flanking sequences only by DSC. A C-terminal PISP extension does not exert a significant effect on the T_m relative to PR/DRV (<2 °C, Figure 2C and Table 1). This observation is consistent with a previous finding that a partial RT sequence (19 amino acids) fused to the C-terminus of PR had an insignificant effect on dimerization,[2] and catalytic activity is not compromised even when attached to the full-length RT.[2,33,35] However, addition of N-terminal extensions to PR^{PISP} decreases the T_m of its ternary complexes with DRV (cf. Table 1, column 4) to a significantly smaller extent than that observed on N-terminal extension of PR alone. Interestingly, however, unlike our observations with PR (Figure 2C and Table 1), the destabilization of PR^{PISP} by N-terminal extensions appears not to depend on the length of the extension, as it is very similar (only 1 °C difference) for ^{SFNF}PR^{PISP} and TFR-PR^{PISP}. Notably, addition of C-terminal PISP (as its DRV complex) partially offsets (by 5−10 °C) the thermal destabilization of PR/DRV that results from an N-terminal extension, although it has little effect on the T_m of PR/DRV by itself. The exact mechanism of this effect is unclear in the absence of structural information.

Concluding Remarks. The precise onset of mature PR activity in the life cycle of HIV is crucial for its assembly and maturation.[2,3] Structural and calorimetric analyses of PR

dx.doi.org/10.1021/bi201809s | Biochemistry 2012, 51, 1041−1050

precursor analogues presented here give further insights into a model for the regulation of PR which releases itself from its precursor Gag-Pol via cleavages at its termini to form a stable dimer held together mainly through interactions of residues at the active site and the termini. Prior to its cleavage at the N-terminus, PR precursor exhibits negligible activity because the dimer to monomer equilibrium constant is high. The present findings indicate that the intrinsic high K_d of the PR precursor is mainly due to a perturbed terminal dimer interface capable of forming at least the inner 2-stranded β-sheet through interactions of the C-terminal residues and possibly lacking the β-sheet interactions of its N-terminal residues. Our observed partial disengagement of the N-terminal strand from the β-sheet interface in two independent ^{SFNF}PR–PI (DRV or SQV) complexes is consistent with a proposed intramolecular mechanism of N-terminal autoprocessing in which the disengaged strand containing the Phe-Pro cleavage site is mobile and capable of accessing the active site of the same molecule. We envision that two distal cleavages (sites 1 and 2 in Figure 1) that likely precede the TFR/PR site at pH below 6 could occur by a similar mechanism via transient dimers. The intramolecular process that dominates the initial part of the N-terminal autoprocessing reaction may become competitive with an intermolecular process (one PR dimer cleaving the N-termini of another dimer) once sufficient active protease (stable dimers) accumulates. Thus, the TFR may mimic the role of a proregion, under specific conditions, similar to that seen with eukaryotic aspartic proteases as in pepsinogen conversion to pepsin.[36,37] Overall, deletion and insertion analyses of TFR emphasize the fact that the full-length TFR with its native cleavage sites is critical for the regulated processing of PR from the Gag-Pol and optimal catalytic activity.[3]

Failure to observe significant differences in PI interactions with ^{SFNF}PR as compared to PR implies that weaker binding of PIs DRV and SQV is likely a consequence of dimer destabilization in ^{SFNF}PR. Ongoing studies of the PR and its multi-drug-resistant mutants fused to longer flanking sequences of the TFR as well as with much weaker binding substrate-like inhibitors may help to reveal differences in the inhibitor-mediated dimer interface interactions at the active site and further differences at the terminal β-sheet between the mature PR and its precursor. The unique (likely transient) terminal β-sheet conformations presented here may enable defining a novel class of inhibitors to perturb dimerization of PR by targeting the interior of the interface formed by the C-terminal residues prior to its autocatalytic maturation from the Gag-Pol. In this context, putative dimerization inhibitors designed for the mature PR with the potential to perturb the interactions between the C-terminal residues may prove more effective as inhibitors of autoprocessing in light of the much weaker terminal interface of the precursor. Defining reagents that selectively interact with the PR upon its N-terminal autoprocessing may aid in screening for inhibitors that block the folding and dimerization of the PR precursor. Recent methodologies such as generating biologically active peptides using bacterial systems could be applied to target the protease precursor.[38]

■ ASSOCIATED CONTENT

Accession Codes

The atomic coordinates and structure factors have been deposited in the Protein Data Bank as entries 3TKW (^{SFNF}PR/DRV), 3TL9 (^{SFNF}PR/SQV), and 3TKG (^{SFNF}PR/SQV_{2dimer}).

■ AUTHOR INFORMATION

Corresponding Author

*Tel 301 594-3122; Fax 301 480-4001; e-mail johnl@intra.niddk.nih.gov.

Author Contributions

[§]These authors contributed equally to the experimental work.

Funding

This research was supported by the Intramural Research Program of the NIDDK, National Institutes of Health and the Intramural AIDS-Targeted Antiviral Program of the Office of the Director, NIH, and grant GM062920 from the NIH.

■ ACKNOWLEDGMENTS

We thank Annie Aniana for excellent technical assistance. We are grateful to Dennis A. Torchia for reading and conveying critical comments. PIs used in this study were obtained through the NIH AIDS Research and Reference Reagent Program, Division of AIDS, NIAID, NIH.

■ ABBREVIATIONS

HIV-1, human immunodeficiency virus type 1; PR, mature HIV-1 protease; TFR, transframe region of the Gag-Pol precursor; PIs, clinical inhibitors of HIV-1 protease; DRV, darunavir; SQV, saquinavir; DSC, differential scanning calorimetry; ITC, isothermal titration calorimetry; K_d, dimer dissociation constant; K_i, inhibitor dissociation constant.

■ REFERENCES

(1) Oroszlan, S., and Luftig, R. B. (1990) Retroviral proteinases. *Curr. Top. Microbiol. Immunol. 157*, 153–185.

(2) Louis, J. M., Weber, I. T., Tozser, J., Clore, G. M., and Gronenborn, A. M. (2000) HIV-1 protease: maturation, enzyme specificity, and drug resistance. *Adv. Pharmacol. 49*, 111–146.

(3) Louis, J. M., Ishima, R., Torchia, D. A., and Weber, I. T. (2007) HIV-1 Protease: Structure, Dynamics, and Inhibition. *Adv. Pharmacol. 55*, 261–298.

(4) Todd, M. J., Semo, N., and Freire, E. (1998) The structural stability of the HIV-1 protease. *J. Mol. Biol. 283*, 475–488.

(5) Johnson, V. A., Brun-Vezinet, F., Clotet, B., Gunthard, H. F., Kuritzkes, D. R., Pillay, D., Schapiro, J. M., and Richman, D. D. (2010) Update of the drug resistance mutations in HIV-1: December 2010. *Top. HIV Med. 18*, 156–163.

(6) Agniswamy, J., and Weber, I. T. (2009) HIV-1 Protease: Structural perspectives on drug resistance. *Viruses 1*, 1110–1136.

(7) Sluis-Cremer, N., and Tachedjian, G. (2002) Modulation of the oligomeric structures of HIV-1 retroviral enzymes by synthetic peptides and small molecules. *Eur. J. Biochem. 269*, 5103–5111.

(8) Cardinale, D., Salo-Ahen, O. M., Ferrari, S., Ponterini, G., Cruciani, G., Carosati, E., Tochowicz, A. M., Mangani, S., Wade, R. C., and Costi, M. P. (2010) Homodimeric enzymes as drug targets. *Curr. Med. Chem. 17*, 826–846.

(9) Haraguchi, H., Sudo, S., Noda, T., Momose, F., Kawaoka, Y., and Morikawa, Y. (2010) Intracellular localization of human immunodeficiency virus type 1 Gag and GagPol products and virus particle release: relationship with the Gag-to-GagPol ratio. *Microbiol. Immunol. 54*, 734–746.

(10) Tang, C., Louis, J. M., Aniana, A., Suh, J. Y., and Clore, G. M. (2008) Visualizing transient events in amino-terminal autoprocessing of HIV-1 protease. *Nature 455*, 693–696.

(11) Tessmer, U., and Krausslich, H. G. (1998) Cleavage of human immunodeficiency virus type 1 proteinase from the N- terminally

adjacent p6* protein is essential for efficient Gag polyprotein processing and viral infectivity. *J. Virol. 72*, 3459−3463.
(12) Pettit, S. C., Everitt, L. E., Choudhury, S., Dunn, B. M., and Kaplan, A. H. (2004) Initial cleavage of the human immunodeficiency virus type 1 GagPol precursor by its activated protease occurs by an intramolecular mechanism. *J. Virol. 78*, 8477−8485.
(13) Louis, J. M., Aniana, A., Weber, I. T., and Sayer, J. M. (2011) Inhibition of autoprocessing of natural variants and multidrug resistant mutant precursors of HIV-1 protease by clinical inhibitors. *Proc. Natl. Acad. Sci. U. S. A. 108*, 9072−9077.
(14) Beissinger, M., Paulus, C., Bayer, P., Wolf, H., Rosch, P., and Wagner, R. (1996) Sequence-specific resonance assignments of the ^{1}H-NMR spectra and structural characterization in solution of the HIV-1 transframe protein p6. *Eur. J. Biochem. 237*, 383−392.
(15) Leiherer, A., Ludwig, C., and Wagner, R. (2009) Uncoupling human immunodeficiency virus type 1 Gag and Pol reading frames: role of the transframe protein p6* in viral replication. *J. Virol. 83*, 7210−7220.
(16) Paulus, C., Hellebrand, S., Tessmer, U., Wolf, H., Krausslich, H. G., and Wagner, R. (1999) Competitive inhibition of human immunodeficiency virus type-1 protease by the Gag-Pol transframe protein. *J. Biol. Chem. 274*, 21539−21543.
(17) Huang, L., Li, Y., and Chen, C. (2011) Flexible catalytic site conformations implicated in modulation of HIV-1 protease autoprocessing reactions. *Retrovirology 8*, 79.
(18) Sayer, J. M., Agniswamy, J., Weber, I. T., and Louis, J. M. (2010) Autocatalytic maturation, physical/chemical properties, and crystal structure of group N HIV-1 protease: relevance to drug resistance. *Protein Sci. 19*, 2055−2072.
(19) Ishima, R., Torchia, D. A., and Louis, J. M. (2007) Mutational and structural studies aimed at characterizing the monomer of HIV-1 protease and its precursor. *J. Biol. Chem. 282*, 17190−17199.
(20) Sayer, J. M., Liu, F., Ishima, R., Weber, I. T., and Louis, J. M. (2008) Effect of the active-site D25N mutation on the structure, stability and ligand binding of the mature HIV-1 protease. *J. Biol. Chem. 283*, 13459−13470.
(21) Otwinowski, Z., and Minor, W. (1997) Processing of x-ray diffraction data in oscillation mode. *Methods Enzymol. 276*, 307−326.
(22) Storoni, L. C., McCoy, A. J., and Read, R. J. (2004) Likelihood-enhanced fast rotation functions. *Acta Crystallogr., Sect. D: Biol. Crystallogr. 60*, 432−438.
(23) McCoy, A. J., Grosse-Kunstleve, R. W., Storoni, L. C., and Read, R. J. (2005) Likelihood-enhanced fast translation functions. *Acta Crystallogr., Sect. D: Biol. Crystallogr. 61*, 458−464.
(24) Tie, Y., Boross, P. I., Wang, Y. F., Gaddis, L., Hussain, A. K., Leshchenko, S., Ghosh, A. K., Louis, J. M., Harrison, R. W., and Weber, I. T. (2004) High resolution crystal structures of HIV-1 protease with a potent non-peptide inhibitor (UIC-94017) active against multi-drug-resistant clinical strains. *J. Mol. Biol. 338*, 341−352.
(25) Tie, Y., Kovalevsky, A. Y., Boross, P., Wang, Y. F., Ghosh, A. K., Tozser, J., Harrison, R. W., and Weber, I. T. (2007) Atomic resolution crystal structures of HIV-1 protease and mutants V82A and I84V with saquinavir. *Proteins 67*, 232−242.
(26) Sheldrick, G. M., and Schneider, T. R. (1997) SHELXL: high resolution refinement. *Methods Enzymol. 277*, 319−343.
(27) Emsley, P., and Cowtan, K. (2004) Coot: model-building tools for molecular graphics. *Acta Crystallogr., Sect. D: Biol. Crystallogr. 60*, 2126−2132.
(28) Laskowski, R. A., MacArthur, M. W., Moss, D. S., and Thornton, J. M. (1993) PROCHECK - a program to check the stereochemical quality of protein structures. *J. Appl. Crystallogr. 26*, 283−291.
(29) Pettersen, E. F., Goddard, T. D., Huang, C. C., Couch, G. S., Greenblatt, D. M., Meng, E. C., and Ferrin, T. E. (2004) UCSF Chimera--a visualization system for exploratory research and analysis. *J. Comput. Chem. 25*, 1605−1612.
(30) Louis, J. M., Clore, G. M., and Gronenborn, A. M. (1999) Autoprocessing of HIV-1 protease is tightly coupled to protein folding. *Nat. Struct. Biol. 6*, 868−875.
(31) Choudhury, S., Everitt, L., Pettit, S. C., and Kaplan, A. H. (2003) Mutagenesis of the dimer interface residues of tethered and untethered HIV-1 protease result in differential activity and suggest multiple mechanisms of compensation. *Virology 307*, 204−212.
(32) Nishitsuji, H., Yokoyama, M., Sato, H., Yamauchi, S., and Takaku, H. (2011) Identification of amino acid residues in HIV-1 reverse transcriptase that are critical for the proteolytic processing of Gag-Pol precursors. *FEBS Lett. 585*, 3372−3377.
(33) Sluis-Cremer, N., Arion, D., Abram, M. E., and Parniak, M. A. (2004) Proteolytic processing of an HIV-1 pol polyprotein precursor: insights into the mechanism of reverse transcriptase p66/p51 heterodimer formation. *Int. J. Biochem. Cell Biol. 36*, 1836−1847.
(34) Tachedjian, G., Moore, K. L., Goff, S. P., and Sluis-Cremer, N. (2005) Efavirenz enhances the proteolytic processing of an HIV-1 pol polyprotein precursor and reverse transcriptase homodimer formation. *FEBS Lett. 579*, 379−384.
(35) Cherry, E., Liang, C., Rong, L., Quan, Y., Inouye, P., Li, X., Morin, N., Kotler, M., and Wainberg, M. A. (1998) Characterization of human immunodeficiency virus type-1 (HIV-1) particles that express protease-reverse transcriptase fusion proteins. *J. Mol. Biol. 284*, 43−56.
(36) Khan, A. R., and James, M. N. (1998) Molecular mechanisms for the conversion of zymogens to active proteolytic enzymes. *Protein Sci. 7*, 815−836.
(37) al-Janabi, J., Hartsuck, J. A., and Tang, J. (1972) Kinetics and mechanism of pepsinogen activation. *J. Biol. Chem. 247*, 4628−4632.
(38) Young, T. S., Young, D. D., Ahmad, I., Louis, J. M., Benkovic, S. J., and Schultz, P. G. (2011) Evolution of cyclic peptide protease inhibitors. *Proc. Natl. Acad. Sci. U. S. A. 108*, 11052−11056.